Earthquakes and Structures, Vol. 4, No. 4 (2013) 341-363
DOI: http://dx.doi.org/10.12989/eas.2013.4.4.341

Modified complex mode superposition design response spectrum method and parameters optimization for linear seismic base-isolation structures

Dong-Mei Huang*[1,2], Wei-Xin Ren[1,2] and Yun Mao[3]

[1]*School of Civil Engineering, Central South University , Changsha, Hunan ,410075 ,China*
[2]*National Engineering Laboratory for High Speed Railway Construction, Central South University, Changsha, Hunan, 410075, China*
[3]*Department of Civil Engineering, Hubei University of Technology, Hubei, Wuhan, China*

(Received March 12, 2012, Revised May 20, 2012, Accepted July 11, 2012)

Abstract. Earthquake response calculation, parametric analysis and seismic parameter optimization of base-isolated structures are some critical issues for seismic design of base-isolated structures. To calculate the earthquake responses for such non-symmetric and non-classical damping linear systems and to implement the earthquake resistant design codes, a modified complex mode superposition design response spectrum method is put forward. Furthermore, to do parameter optimization for base-isolation structures, a graphical approach is proposed by analyzing the relationship between the base shear ratio of a seismic base-isolation floor to non-seismic base-isolation one and frequency ratio-damping ratio, as well as the relationship between the seismic base-isolation floor displacement and frequency ratio-damping ratio. In addition, the influences of mode number and site classification on the seismic base-isolation structure and corresponding optimum parameters are investigated. It is demonstrated that the modified complex mode superposition design response spectrum method is more precise and more convenient to engineering applications for utilizing the damping reduction factors and the design response spectrum, and the proposed graphical approach for parameter optimization of seismic base-isolation structures is compendious and feasible.

Keywords: seismic base-isolation; modified complex modes superposition response spectrum method; graphical approach; parameter optimization; earthquake response

1. Introduction

Base isolation is an anti-seismic technology that can significantly reduce the seismic responses of a superstructure by setting seismic base-isolation devices to extend the system natural period and to increase the system damping (Buckle and Mayes 1990, Skinner *et al.* 1993, Hong and Kim 2004, Fan *et al.* 1991, Naeim and Kelly 1999, Komodromos 2000, Eurocode 2004, Takewaki 2008). At present, there are three main methods to calculate the earthquake responses of seismic base-isolation structures. One is the time domain method that takes a typical seismic wave as the

*Corresponding author, Professor, E-mail: hdm76512@163.com

seismic excitation to calculate the seismic responses in time domain (Heaton *et al.* 1995, Matsagar and Jangid 2004). The second is the frequency domain method that takes the random earthquake ground motion model as the seismic excitation to calculate the random seismic responses in frequency domain (Constantinou and Tadjbakhsh 1983, Jangid and Datta 1995, Takewaki and Fujita 2009). The third is the mode decomposition response spectrum method that calculates the maximum seismic responses according to the mode decomposition and design response spectrum (GB50011-2010) (Igusa *et al.* 1984, Gupta and Jaw 1986, Mahendra and Barbara 1986, Yang *et al.* 1990, Zhou *et al.* 2004).

The time domain method which adopts only one seismic wave as an excitation is difficult to reflect the statistical characteristics as the earthquake is a random process. The frequency method which adopts the seismic random model as an excitation is uncertain for the uncertainties in the model parameters. The mode decomposition response spectrum method, on the other hand, is on the basis of design response spectrum, which is a statistical result according to hundreds of seismic wave excitations and is adopted by the earthquake resistant design code (GB50011-2010) for engineering application. As is well-known, the seismic base-isolation structure is a non-symmetric and non-classical damping system, therefore, the forced real mode decomposition response spectrum method should be substituted by the complex mode superposition design response spectrum method for more accurate results.

With a wide use of seismic base-isolation structures, the parameter optimization design on the seismic base-isolation devices is of interest (Alessandro and Ileana 2004, Zhou and Han 1996, Constantinou and Tadjbakhsh 1984, Cenk and Henri 2004, Takewaki 2005). Nowadays, many constrained optimization methods for parameter optimization have been proposed such as conjugate gradient methods (Horisberger and Belanger 1974), mathematical programming approach (Balling *et al*. 1983), genetic algorithm (Yoshi *et al.* 1999), GA-fuzzy optimization method (Hyun and Paul 2007) and so on. All these methods are performed by constant iterating, which are either time-consuming or non-intuitive. In this paper, a modified complex mode superposition design response spectrum method is implemented to calculate the seismic responses and a graphical approach for parameter optimization of the seismic base-isolation devices is proposed. Moreover, the influences of mode number and site classification on the seismic base-isolation structure and corresponding optimum parameters are investigated.

2. Modified complex modes superposition design response spectrum method

2.1 Motion equation and solution

To calculate the earthquake responses of seismic base-isolation structures, the computational model that not only reflects the actual deformation behavior but also makes the calculation easy and feasible must be set up. At present, the commonly used computational models are a series of multi-particle system model and spatial finite element model. The series of multi-particle system model is herein adopted as shown in Fig. 1. In the figure, the *i*th floor mass of structure is m_i and the mass of structural base plate is m_b, while the stiffness and damping coefficients of seismic base-isolation device are k_b and c_b, respectively. Under the earthquake action, the structural linear motion equation is

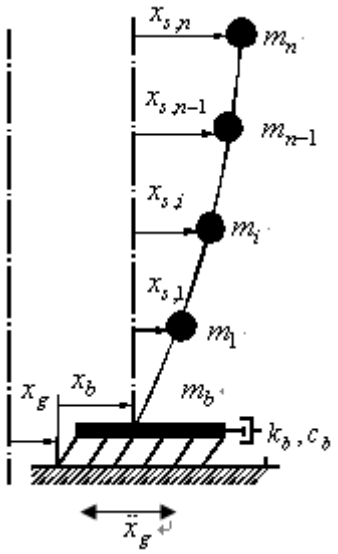

Fig. 1 Motion model for seismic base-isolated structure

$$[M_0]\{\ddot{x}_s\}+[C_0]\{\dot{x}_s\}+[K_0]\{x_s\}=-[M_0]\{I\}\left(\ddot{x}_g+\ddot{x}_b\right) \tag{1a}$$

$$\sum_{i=1}^{n} m_i(\ddot{x}_b+\ddot{x}_{s,i}+\ddot{x}_g)+m_b(\ddot{x}_b+\ddot{x}_g)+c_b\dot{x}_b+k_b x_b=0 \tag{1b}$$

where $\ddot{x}_g$ is the horizontal ground earthquake acceleration; x_b is the displacement of structural base plate; $x_{s,i}$ is the *i*th floor displacement of the structure relative to structural base plate; $[M_0]$ is the lumped mass matrix of superstructure; $[K_0]=[k_{ij}]=[\delta_{ij}]^{-1}$ is the lateral stiffness matrix of superstructure, which is obtained according to the mechanical meanings of stiffness coefficient k_{ij} or flexibility coefficient δ_{ij}; $[C_0]$ is the damping matrix of superstructure with Rayleigh Damping; $\{I\}=[1,1,\cdots,1]^{\mathrm{T}}$.

Let

$$\{x_s\}=[x_{s,1},x_{s,2},\cdots,x_{s,i},\cdots x_{s,n},]^{\mathrm{T}}=\sum_{j=1}^{m} q_j\{\varphi_j\} \tag{2}$$

$$\{\varphi_j\}=\{\varphi_{1j},\cdots,\varphi_{ij},\cdots,\varphi_{nj}\}^{\mathrm{T}}$$

where *m* is the number of modes for combination. Eq. (1) can be transformed into the following by the modal decomposition

$$\ddot{q}_j + \gamma_j \ddot{x}_b + 2\xi_j \omega_j \dot{q}_j + \omega_j^2 q_j = -\gamma_j \ddot{x}_g \quad (j = 1 \sim m) \tag{3a}$$

$$\sum_{j=1}^{m} \alpha_j \ddot{q}_j + (1+\psi_1)\ddot{x}_b + 2\xi_b \omega_b \dot{x}_b + \omega_b^2 x_b = -(1+\psi_1)\ddot{x}_g \tag{3b}$$

in which

$$M_j^* = \{\varphi_j\}^{\mathrm{T}} [M_0] \{\varphi_j\}; \quad K_j^* = \{\varphi_j\}^{\mathrm{T}} [K_0] \{\varphi_j\}; \quad C_j^* = \{\varphi_j\}^{\mathrm{T}} [C_0] \{\varphi_j\}$$

$$2\xi_j \omega_j = C_j^* / M_j^*; \quad \omega_j^2 = K_j^* / M_j^*; \quad 2\xi_b \omega_b = c_b / m_b; \quad \omega_b^2 = k_b / m_b$$

$$\gamma_j = (\sum_{i=1}^{n} m_i \varphi_{ij}) \Big/ (\sum_{i=1}^{n} m_i \varphi_{ij}^2); \quad \psi_1 = (\sum_{i=1}^{n} m_i) \Big/ m_b; \quad \alpha_j = (\sum_{i=1}^{n} m_i \varphi_{ij}) \Big/ m_b$$

Let $\{\tilde{x}\} = [q_1, q_2, \cdots, q_n, x_b]^{\mathrm{T}}$, then Eq. (3) can be deduced to the following unified form

$$[\tilde{M}]\{\ddot{\tilde{x}}\} + [\tilde{C}]\{\dot{\tilde{x}}\} + [\tilde{K}]\{\tilde{x}\} = \{\tilde{f}(t)\} \tag{4}$$

in which

$$[\tilde{M}] = \begin{bmatrix} 1 & 0 & \cdots & 0 & \gamma_1 \\ 0 & 1 & 0 & \cdots & \gamma_2 \\ \cdots & \cdots & \cdots & \cdots & \cdots \\ 0 & 0 & \cdots & 1 & \gamma_m \\ \alpha_1 & \alpha_2 & \cdots & \alpha_m & 1+\psi_1 \end{bmatrix}; \quad [\tilde{C}] = \begin{bmatrix} 2\xi_1\omega_1 & & & & \\ & 2\xi_2\omega_2 & & 0 & \\ & & \ddots & & \\ & 0 & & 2\xi_m\omega_m & \\ & & & & 2\xi_b\omega_b \end{bmatrix};$$

$$[\tilde{K}] = \begin{bmatrix} \omega_1^2 & & & & \\ & \omega_2^2 & & 0 & \\ & & \ddots & & \\ & 0 & & \omega_m^2 & \\ & & & & \omega_b^2 \end{bmatrix}; \quad \{\tilde{f}(t)\} = -\ddot{x}_g [\gamma_1, \gamma_2, \cdots, \gamma_m, 1+\psi_1]^{\mathrm{T}}$$

The damping matrix in Eq. (4) is composed of structural damping and additional damping of base-isolation devices, which is a non-classical large damping matrix. As a result, the mass matrix is a non-symmetric matrix. Eq. (4) can be decoupled by the complex modes.
Let

$$\{y\} = [y_1, y_2, ..., y_{2(m+1)}]^T = [\dot{q}_1, ..., \dot{q}_m, \dot{x}_b, q_1, ..., q_m, x_b]^T \tag{5}$$

Then Eq. (4) can be deduced to the following unified form

$$[M]\{\dot{y}\}+[K]\{y\}=\{f(t)\} \tag{6}$$

in which

$$[M]=\begin{bmatrix}[0] & [\tilde{M}]\\ [\tilde{M}] & [\tilde{C}]\end{bmatrix},\ [K]=\begin{bmatrix}-[\tilde{M}] & [0]\\ [0] & [\tilde{K}]\end{bmatrix}$$

$$\{f(t)\}=-\ddot{x}_g[0,\cdots,0,\gamma_1,\cdots,\gamma_m,1+\psi_1]^{\mathrm{T}}_{2(m+1)\times 1}$$

The 2(*m*+1) eigenvalues p_k ($k=1\sim 2(m+1)$) can be obtained by solving the eigenvalue equation $|p[M]+[K]|=0$, and their corresponding right and left eigenvector equations are as follows

$$[D(p_k)]\{U_k\}=\{0\};\ [D(p_k)]^{\mathbf{T}}\{V_k\}=\{0\}\quad (k=1\sim 2(m+1)) \tag{7}$$

Each corresponding right and left eigenvectors of p_k are

$$\{U_k\}=[U_{1k},U_{2k},\cdots,U_{2(m+1)k}]^{\mathbf{T}},\ \{V_k\}=[V_{1k},V_{2k},\cdots,V_{2(m+1)k}]^{\mathbf{T}} \tag{8}$$

Accordingly, $[P]=diag[p_k]$ ($k=1\sim 2(m+1)$), $[U]=[U_1,U_2,\cdots,U_{2(m+1)}]$, and $[V]=[V_1,V_2,\cdots,V_{2(m+1)}]$ are called the eigenvalue matrix, right eigenvector matrix, and left eigenvector matrix, respectively. The system meets with the following weighted orthogonality (Fawzy and Bishop 1976)

$$[V]^{\mathbf{T}}[M][U]=diag[m_k^*];\ [V]^{\mathbf{T}}[K][U]=-diag[m_k^*]\ [P] \tag{9}$$

By means of the transformation $\{y\}=[U]\{z\}$ and orthogonality, Eq. (6) can be decoupled to

$$\{\dot{z}\}-[P]\{z\}=\{F(t)\} \tag{10}$$

in which $\{F(t)\}=[\mu][V]^{\mathrm{T}}\{f(t)\}$; $[\mu]=diag[\mu_k]=diag[m_k^{*-1}]$. The component form of Eq. (10) is

$$\dot{z}_k-p_kz_k=R_k\ddot{x}_g\quad (k=1\sim 2(m+1)) \tag{11}$$

where $R_k=-\mu_k\{V_k\}^{\mathrm{T}}[0,\cdots,0,\gamma_1,\cdots,\gamma_m,1+\psi_1]^{\mathrm{T}}_{2(m+1)\times 1}$. The solution of Eq. (11) is

$$z_k(t)=R_k\int_0^t\ddot{x}_g(\tau)e^{p_k(t-\tau)}\mathrm{d}\tau\quad (k=1\sim 2(m+1)) \tag{12}$$

According to the transformation Eq. (5) and the complex modal transformation $\{y\}=[U]\{z\}$, the generalized coordinates and the displacement of structural base plate are

$$q_j=\sum_{k=1}^{2(m+1)}\phi_{jk}z_k=\sum_{k=1}^{2(m+1)}\phi_{jk}R_k\int_0^t\ddot{x}_g(\tau)e^{p_k(t-\tau)}\mathrm{d}\tau \quad (j=1\sim m) \tag{13a}$$

$$x_b=\sum_{k=1}^{2(m+1)}\phi_{(m+1)k}z_k=\sum_{k=1}^{2(m+1)}\phi_{(m+1)k}R_k\int_0^t\ddot{x}_g(\tau)e^{p_k(t-\tau)}\mathrm{d}\tau \tag{13b}$$

where $\{U_k\}=\begin{Bmatrix}p_k\{\phi_k\}\\ \{\phi_k\}\end{Bmatrix}$, $\{\phi_k\}=\left[\phi_{1k},\phi_{2k},\cdots,\phi_{jk},\cdots,\phi_{(m+1)k}\right]^{\mathbf{T}}$

2.2 Complex modes superposition design response spectrum method

As the complex frequencies are conjugated, let $p_k=p_{m+1+k}^*$, then $\{\phi_k\}=\{\phi_{m+1+k}^*\}$ and $R_k=R_{m+1+K}^*$. Because the actual system has a real solution, Eq. (13) can then be expressed as

$$q_j=2\sum_{k=1}^{m+1}\mathrm{Re}[\phi_{jk}R_k\int_0^t\ddot{x}_g(\tau)e^{p_k(t-\tau)}\mathrm{d}\tau] \quad (j=1\sim m) \tag{14a}$$

$$x_b=2\sum_{k=1}^{m+1}\mathrm{Re}[\phi_{(m+1)k}z_k]=2\sum_{k=1}^{m+1}\mathrm{Re}[\phi_{(m+1)k}R_k\int_0^t\ddot{x}_g(\tau)e^{p_k(t-\tau)}\mathrm{d}\tau] \tag{14b}$$

Let

$$p_k=-A_k+iD_k=-\tilde{\xi}_k\tilde{\omega}_k+i\tilde{\omega}_k\sqrt{1-\tilde{\xi}_k^2} \tag{15}$$

$$(k=1\sim m+1, i=\sqrt{-1})$$

Then

$$\tilde{\omega}_k=|p_k|=\sqrt{A_k^2+D_k^2}\ ;\ \ \tilde{\xi}_k=-\mathrm{Re}(p_k)/\tilde{\omega}_k=\frac{A_k}{\sqrt{A_k^2+D_k^2}} \tag{16}$$

where $\tilde{\xi}_k$ is the *k*th generalized damping ratio and $\tilde{\omega}_k$ is the *k*th complex frequency.

Substituting Eq. (16) into Eq. (14) yields

$$q_j=2\sum_{k=1}^{m+1}\mathrm{Re}[(\phi_{jk}R_k\int_0^t\ddot{x}_g(\tau)e^{-\tilde{\xi}_k\tilde{\omega}_k(t-\tau)}e^{i\tilde{\omega}_k\sqrt{1-\tilde{\xi}_k^2}(t-\tau)}\mathrm{d}\tau] \quad (j=1\sim m) \tag{17a}$$

$$x_b = 2\sum_{k=1}^{m+1} \mathrm{Re}[\phi_{(m+1)k} R_k \int_0^t \ddot{x}_g(\tau) e^{-\tilde{\xi}_k \tilde{\omega}_k (t-\tau)} e^{i\tilde{\omega}_k \sqrt{1-\tilde{\xi}_k^2}(t-\tau)} \mathrm{d}\tau] \tag{17b}$$

By implementing the Euler equations $e^{\pm i\theta} = \cos\theta \pm i \sin\theta$, Eq. (17) becomes

$$q_j = 2\sum_{k=1}^{m+1} \mathrm{Re}[(\phi_{jk} R_k \int_0^t \ddot{x}_g(\tau) e^{-\tilde{\xi}_k \tilde{\omega}_k (t-\tau)} \cos\tilde{\omega}_{Dk}(t-\tau)\mathrm{d}\tau$$

$$+\phi_{jk} R_k i \int_0^t \ddot{x}_g(\tau) e^{-\tilde{\xi}_k \tilde{\omega}_k (t-\tau)} \sin\tilde{\omega}_{Dk}(t-\tau)\mathrm{d}\tau] \tag{18a}$$

$$x_b = 2\sum_{k=1}^{m+1} \mathrm{Re}[\phi_{(m+1)k} R_k \int_0^t \ddot{x}_g(\tau) e^{-\tilde{\xi}_k \tilde{\omega}_k (t-\tau)} \cos\tilde{\omega}_{Dk}(t-\tau)\mathrm{d}\tau$$

$$+\phi_{(m+1)k} R_k i \int_0^t \ddot{x}_g(\tau) e^{-\tilde{\xi}_k \tilde{\omega}_k (t-\tau)} \sin\tilde{\omega}_{Dk}(t-\tau)\mathrm{d}\tau] \tag{18b}$$

where $\tilde{\omega}_{Dk} = \tilde{\omega}_k \sqrt{1-\tilde{\xi}_k^2}$

In order to solve the Eq. (18) further, a single degree of freedom system is discussed firstly. The motion equation of a system with a single degree of freedom under seismic excitation is

$$\ddot{\eta}_k + 2\tilde{\xi}_k \tilde{\omega}_k \dot{\eta}_k + \tilde{\omega}_k^2 \eta_k = -\ddot{x}_g \tag{19}$$

By the Duhamel integral the solution is

$$\eta_k = \frac{-1}{\tilde{\omega}_{Dk}} \int_0^t \ddot{x}_g(\tau) e^{-\tilde{\xi}_k \tilde{\omega}_k (t-\tau)} \sin\tilde{\omega}_{Dk}(t-\tau)\mathrm{d}\tau \tag{20}$$

The derivation of the above solution is

$$\dot{\eta}_k = -\tilde{\xi}_k \tilde{\omega}_k \eta_k - \int_0^t \ddot{x}_g(\tau) e^{-\tilde{\xi}_k \tilde{\omega}_k (t-\tau)} \cos\tilde{\omega}_{Dk}(t-\tau)\mathrm{d}\tau \tag{21}$$

By using Eqs. (20) and (21), Eq. (18) becomes

$$q_j = 2\sum_{k=1}^{m+1} \mathrm{Re}\left\{(\phi_{jk} R_k \left[\tilde{\xi}_k \tilde{\omega}_k + \tilde{\omega}_{Dk} i\right] \cdot \eta_k + \phi_{jk} R_k \cdot \dot{\eta}_k\right\} \quad (j = 1 \sim m) \tag{22a}$$

$$x_b = 2\sum_{k=1}^{m+1} \mathrm{Re}\left\{\phi_{(m+1)k} R_k \left[\tilde{\xi}_k \tilde{\omega}_k + \tilde{\omega}_{Dk} i\right] \cdot \eta_k + \phi_{(m+1)k} R_k \cdot \dot{\eta}_k\right\} \tag{22b}$$

Let $h_{jk} = \phi_{jk} R_k [\tilde{\xi}_k \tilde{\omega}_k + \tilde{\omega}_{Dk} i] = E_{jk} + F_{jk} i$, $h'_{jk} = \phi_{jk} R_k = G_{jk} + H_{jk} i$ and

$g_k = \phi_{(m+1)k} R_k [\tilde{\xi}_k \tilde{\omega}_k + \tilde{\omega}_{Dk} i] = \tilde{E}_k + \tilde{F}_k i$, $g'_{jk} = \phi_{(m+1)k} R_k = \tilde{G}_k + \tilde{H}_k i$, Eq. (22) can be converted into

$$q_j = \sum_{k=1}^{m+1} (2E_{jk}\eta_k + 2G_{jk}\dot{\eta}_k) \quad (j = 1 \sim m) \tag{23a}$$

$$x_b = \sum_{k=1}^{m+1} (2\tilde{E}_k \eta_k + 2\tilde{G}_k \dot{\eta}_k) \tag{23b}$$

In order to utilize the design response spectrum of the seismic code, q_j and x_b must be solved by superposition of absolute maximum responses of series of single degree of freedom systems. Assumed that the seismic excitation is a zero mean stationary white noise process and the peak factor is unity, according to the random vibration theory and considering the influence of the cross-term, the absolute maximums of q_j and x_b can be obtained by (the derivation process is shown in Appendix A)

$$\left|q_j\right|_{\max} \text{ or } \left|x_b\right|_{\max} = \sqrt{S_1 + S_2 + S_3} \quad (j = 1 \sim m) \tag{24}$$

in which

$$S_1 = \sum_{k=1}^{m+1} \sum_{l=1}^{m+1} 2E_{jk} \cdot 2E_{jl} \cdot \rho_{kl}^{DD} \cdot S_{dk} \cdot S_{dl} \tag{25a}$$

$$S_2 = 2\sum_{k=1}^{n+1} \sum_{l=1}^{n+1} 2E_{jk} \cdot 2G_{jl} \cdot \rho_{kl}^{VD} \cdot S_{dk} \cdot S_{vl} \tag{25b}$$

$$S_3 = \sum_{k=1}^{n+1} \sum_{l=1}^{n+1} 2G_{jk} \cdot 2G_{jl} \cdot \rho_{kl}^{VV} \cdot S_{dk} \cdot S_{vl} \tag{25c}$$

$$\rho_{kl}^{DD} = 8\sqrt{\tilde{\xi}_k \tilde{\xi}_l \tilde{\omega}_k \tilde{\omega}_l} (\tilde{\xi}_k \tilde{\omega}_k + \tilde{\xi}_l \tilde{\omega}_l) \tilde{\omega}_k \tilde{\omega}_l / \Gamma_{kl} \tag{25d}$$

$$\rho_{kl}^{VD} = 4\sqrt{\tilde{\xi}_k \tilde{\xi}_l \tilde{\omega}_k \tilde{\omega}_l} (\tilde{\omega}_l^2 - \tilde{\omega}_k^2) \tilde{\omega}_l / \Gamma_{kl} \tag{25e}$$

$$\rho_{kl}^{VV} = 8\sqrt{\tilde{\xi}_k \tilde{\xi}_l \tilde{\omega}_k \tilde{\omega}_l} (\tilde{\xi}_k \tilde{\omega}_l + \tilde{\xi}_l \tilde{\omega}_k) \tilde{\omega}_k \tilde{\omega}_l / \Gamma_{kl} \tag{25f}$$

$$\Gamma_{kl} = (\tilde{\omega}_k^2 - \tilde{\omega}_l^2)^2 + 4\tilde{\xi}_k \tilde{\xi}_l \tilde{\omega}_k \tilde{\omega}_l (\tilde{\omega}_k^2 + \tilde{\omega}_l^2) + 4(\tilde{\xi}_k^2 - \tilde{\xi}_l^2) \tilde{\omega}_k^2 \tilde{\omega}_l^2 \tag{25g}$$

where $S_{dk}(S_{dl})$ and $S_{vk}(S_{vl})$ are the absolute maximal displacement and velocity of a single degree of freedom system (Eq. (19)), respectively, i.e., the displacement response spectrum and velocity response spectrum. When it comes to the absolute maximal displacement of seismic

base-isolation floor, i.e. $|x_b|_{\max}$, the E_{jk} and G_{jk} in Eq. (25) are replaced by $\tilde{E}_k$ and $\tilde{G}_k$, respectively .

However, the code for seismic design of buildings (GB50011-2010) does not provide the displacement response spectrum and the velocity response spectrum, except for the corresponding acceleration response spectrum, therefore, the Eq. (25) can't be applied directly and must be further deduced.

As we all know, in the case of small damping ratio such as $\xi = 5\%$, the displacement response spectrum, velocity response spectrum and acceleration response spectrum of a single degree of freedom system have the following approximate relationship

$$S_{d0} : S_{v0} : S_{a0} = 1 : \omega : \omega^2 \tag{26}$$

However, Eq. (26) can't be substituted into Eq. (25) directly for the damping ratio in it is not a small one. Lin and Chang (2003) analyzed the displacement and velocity responses of single degree of freedom systems with different damping ratio excited by 1053 actual earthquake acceleration time-history records and then gave the damping reduction factor derived from the displacement and velocity, respectively, as shown in Table 1, which can be expressed as

$$B_d = \frac{S_d}{S_{d0}}, \quad B_v = \frac{S_v}{S_{v0}} \tag{27}$$

where B_d and B_v are the damping reduction factor derived from the displacement and velocity,

Table 1 Damping reduction factors derived from（a）displacement and（b）velocity

	Damping	Period (s)											
		0.1	0.5	1	2	3	4	5	6	7	8	9	10
(a)	2%/5%	1.25	1.31	1.30	1.28	1.25	1.23	1.21	1.19	1.17	1.15	1.14	1.12
	10%/5%	0.85	0.77	0.78	0.79	0.80	0.80	0.81	0.83	0.84	0.85	0.86	0.87
	15%/5%	0.77	0.65	0.66	0.67	0.69	0.69	0.70	0.72	0.74	0.76	0.77	0.78
	20%/5%	0.72	0.57	0.57	0.59	0.61	0.61	0.63	0.65	0.67	0.69	0.70	0.20
	25%/5%	0.69	0.51	0.51	0.52	0.55	0.56	0.57	0.60	0.62	0.64	0.65	0.68
	30%/5%	0.66	0.46	0.47	0.48	0.51	0.51	0.53	0.56	0.58	0.60	0.61	0.64
	40%/5%	0.61	0.40	0.40	0.41	0.44	0.45	0.46	0.49	0.51	0.54	0.55	0.58
	50%/5%	0.58	0.35	0.35	0.36	0.39	0.40	0.42	0.45	0.47	0.49	0.51	0.54
(b)	2%/5%	1.37	1.31	1.27	1.21	1.16	1.14	1.11	1.09	1.07	1.05	1.04	1.03
	10%/5%	0.77	0.77	0.80	0.84	0.87	0.88	0.90	0.92	0.94	0.95	0.95	0.97
	15%/5%	0.65	0.65	0.69	0.74	0.80	0.82	0.84	0.87	0.90	0.92	0.92	0.94
	20%/5%	0.57	0.57	0.62	0.68	0.74	0.77	0.80	0.84	0.87	0.89	0.90	0.92
	25%/5%	0.52	0.51	0.57	0.63	0.70	0.74	0.77	0.81	0.85	0.87	0.89	0.91
	30%/5%	0.48	0.46	0.52	0.60	0.67	0.71	0.75	0.79	0.83	0.85	0.87	0.90
	40%/5%	0.42	0.39	0.46	0.54	0.62	0.67	0.71	0.76	0.80	0.83	0.85	0.88
	50%/5%	0.37	0.34	0.41	0.50	0.59	0.64	0.68	0.73	0.77	0.80	0.83	0.86

respectively; S_d and S_v are respectively the displacement response spectrum and velocity response spectrum of single degree of freedom system with damping ratio $\xi \neq 5\%$, S_{d0} and S_{v0} are respectively the displacement response spectrum and velocity response spectrum of single degree of freedom system with damping ratio $\xi = 5\%$.

Therefore, S_1, S_2 and S_3 in Eq. (25) can be further deduced as

$$S_1 = \sum_{k=1}^{m+1} \sum_{l=1}^{m+1} 2E_{jk} B_{dk} \cdot 2E_{jl} B_{dl} \cdot \rho_{kl}^{DD} \cdot S_{dk0} \cdot S_{dl0} \tag{28a}$$

$$S_2 = 2\sum_{k=1}^{n+1} \sum_{l=1}^{n+1} 2E_{jk} B_{dk} \cdot 2G_{jl} B_{vl} \cdot \rho_{kl}^{VD} \cdot S_{dk0} \cdot S_{vl0} \tag{28b}$$

$$S_3 = \sum_{k=1}^{n+1} \sum_{l=1}^{n+1} 2G_{jk} B_{vk} \cdot 2G_{jl} B_{vl} \cdot \rho_{kl}^{VV} \cdot S_{dk0} \cdot S_{vl0} \tag{28c}$$

Where S_{dk0}(S_{dl0}) and S_{vk0}(S_{vl0}) are the displacement response spectrum and the velocity response spectrum of kth(lth) single degree of freedom system with damping ratio $\tilde{\xi}_k = 5\%$, respectively; $B_{dk}(B_{dl})$ and $B_{vk}(B_{vl})$ are the kth(lth) damping reduction factors derived from the displacement and velocity, respectively. When it comes to the absolute maximal displacement of seismic base-isolation floor, i.e., $|x_b|_{\max}$, the E_{jk} and G_{jk} in Eq. (25) are replaced by $\tilde{E}_k$ and $\tilde{G}_k$, respectively.

Let

$$\alpha_0 = S_{a0} / g \tag{29}$$

where α_0 is the design response spectrum with damping ratio $\xi = 5\%$, which is also called earthquake affecting coefficient in the code for seismic design of buildings (GB50011-2010) and is shown in Fig. B1 of Appendix B. The maximum value of horizontal seismic influent coefficient appeared in Fig. B1, which is related to earthquake intensity, is shown in Table B1 of Appendix B.

Considering of Eqs. (26) and (29), S_1 , S_2 and S_3 in Eq. (28) can be rewritten as

$$S_1 = \sum_{k=1}^{n+1} \sum_{l=1}^{n+1} 2a_{jk} B_{dk} \cdot 2a_{jl} B_{dl} \cdot \rho_{kl}^{DD} \cdot \frac{g\alpha_{k0}}{\tilde{\omega}_k^2} \cdot \frac{g\alpha_{l0}}{\tilde{\omega}_l^2} \tag{30a}$$

$$S_2 = 2\sum_{k=1}^{n+1} \sum_{l=1}^{n+1} 2a_{jk} B_{dk} \cdot 2c_{jl} B_{vl} \tilde{\omega}_l \cdot \rho_{kl}^{VD} \cdot \frac{g\alpha_{k0}}{\tilde{\omega}_k^2} \cdot \frac{g\alpha_{l0}}{\tilde{\omega}_l^2} \tag{30b}$$

$$S_3 = \sum_{k=1}^{n+1} \sum_{l=1}^{n+1} 2c_{jk} B_{vk} \tilde{\omega}_k \cdot 2c_{jl} B_{vl} \tilde{\omega}_l \cdot \rho_{kl}^{VV} \cdot \frac{g\alpha_{k0}}{\tilde{\omega}_k^2} \cdot \frac{g\alpha_{l0}}{\tilde{\omega}_l^2} \tag{30c}$$

where $\alpha_{k0} = S_{ak0}/g(\alpha_{l0} = S_{al0}/g)$ is the design response spectrum (i.e., earthquake affecting coefficient) of *k*th(*l*th) single degree of freedom system with damping ratio $\tilde{\xi}_k(\tilde{\xi}_l) = 5\%$.

The derived Eq. (30) not only applies the design response spectrum in the code conveniently but also uses the damping reduction factors to consider the large damping ratio, which improves the work in the literature (Zhou *et al.* 2004) greatly.

In such a way, $|q_j|_{\max}(j = 1 \sim m)$ and $|x_b|_{\max}$ can be obtained according to Eq. (30). Once $|q_j|_{\max}$ is known, the *j*th maximum displacement, maximum earthquake action and maximum interlaminar shear force can be determined according to Eq. (2)

$$|\{x_s\}_j|_{\max} = |q_j|_{\max}\{\varphi_j\} \tag{31a}$$

$$|\{F\}_j|_{\max} = [K_0]|\{x_s\}_j|_{\max} \quad \text{or} \quad |F_{ij}|_{\max} = m_i\omega_j^2\varphi_{ij}|q_j|_{\max} \quad (i = 1 \sim n) \tag{31b}$$

$$V_{ij} = \sum_{k=i}^{n}|F_{kj}|_{\max} \quad (i = 1 \sim n) \tag{31c}$$

Ignoring the cross-term, the finer solution can be calculated by Square Root of the Sum of Squares (SRSS) method

$$|RP|_{\max} = \sqrt{\sum_{j=i}^{m} R_j^2} \tag{32}$$

where R_j expresses the *j*th maximum displacement and maximum interlaminar shear force of each structural floor, while $|RP|_{\max}$ expresses the ultimate combination results.

3. Parameter optimization for seismic base-isolation floor

For the numerical application, one 8-story reinforced concrete structure is taken as an example where the 1st and the 2nd floors are the large markets, the 3rd~7th floors are offices, and the top floor is a revolving restaurant. The seismic intensity is *I*=8 degree (0.2 g) and the site class is II. The classification of design earthquake is the 1st group and the characteristic period is T_g=0.35 s. The mass and stiffness of each floor are listed in Table 2. The basic period of the structure is T_1=0.973 (s) and the damping ratio is $\xi = 0.05$. The mass of seismic base-isolation floor is m_b=400000 kg, while the damping ratio of seismic base-isolation floor is within $0.01 \le \xi_b \le 0.2$. The frequency ratio of seismic base-isolation floor is $0.5 \le \omega_b/\omega_1 \le 3.0$.

In order to obtain the best seismic base-isolation effect, the parameter optimization of seismic base-isolation floor has to be carried out, so as to determine three important parameters of seismic base-isolation floor, which is the mass m_b, natural frequency ω_b and damping ratio ξ_b.

Table 2 Structural parameters of building

Floor No.	Mass (kg)	Stiffness (kN/m)	Storey heights (m)
bottom	400000	30000	-
1	220000	250000	4.5
2	300000	250000	4.5
3	270000	350000	3.0
4	270000	350000	3.0
5	270000	350000	3.0
6	270000	350000	3.0
7	270000	350000	3.0
8	130000	220000	4.5

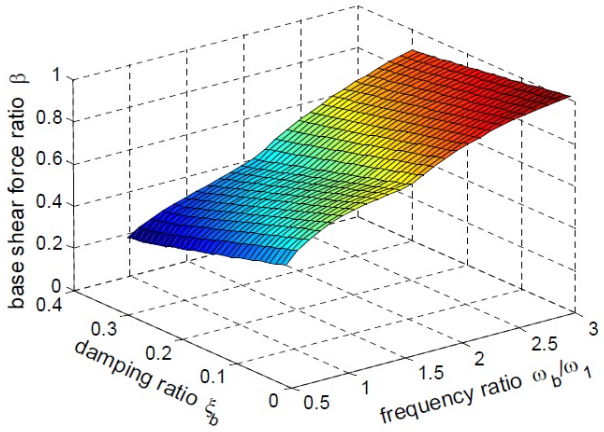

Fig. 2 Base shear force ratio vs. frequency ratios and damping ratios

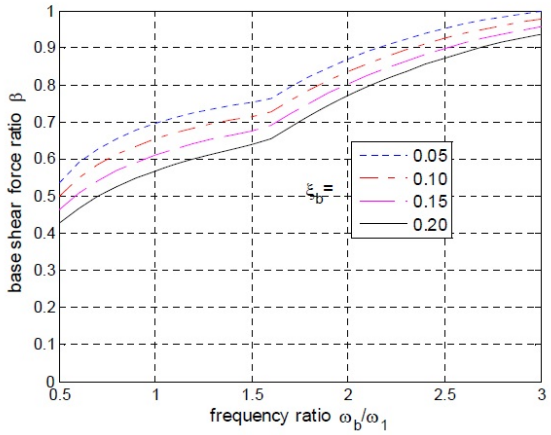

Fig. 3 Base shear force ratio vs. frequency ratio for different damping ratios

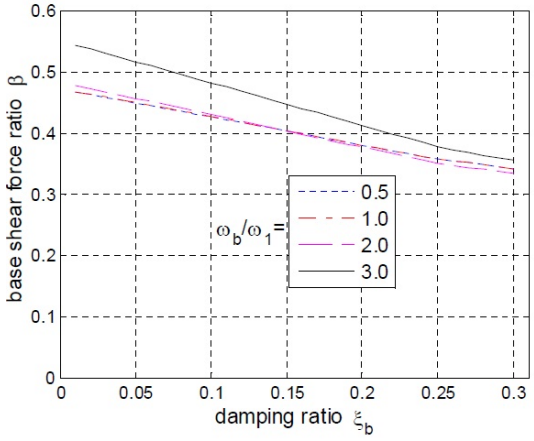

Fig. 4 Base shear force ratio vs. damping ratio for different frequency ratios

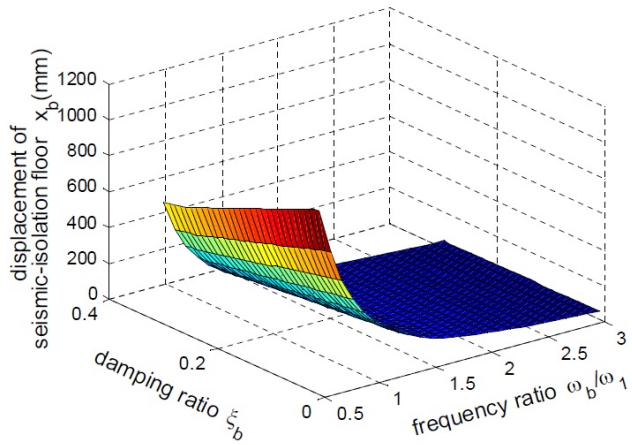

Fig. 5 Seismic base-isolation floor displacement vs. frequency ratios and damping ratios

Supposing that the seismic responses of the structure is mainly contributed by the first mode, when the m_b is known, the base shear of the structure and the displacement of seismic base-isolation floor can be calculated under different frequency ratios ω_b / ω_1 and damping ratios ξ_b. Meanwhile, the base shear of non-seismic-isolation structure can be also calculated by the classical mode decomposition response spectrum method. The relationship between base shear ratio of seismic base-isolation floor to non-seismic base-isolation floor and the frequency ratio, damping ratio is shown in Fig. 2. The relationships between base shear ratio of seismic base-isolation floor to non-seismic base-isolation floor and the frequency ratio under four different damping ratios are shown in Fig. 3. The relationships between base shear ratio of seismic base-isolation floor to non-seismic base-isolation floor and the damping ratio for four different frequency ratios are shown in Fig. 4.

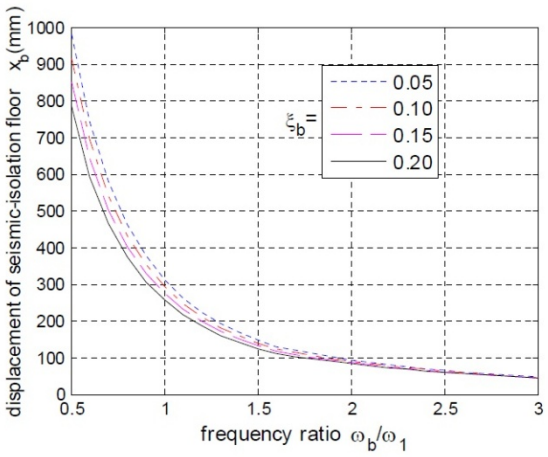

Fig. 6 Seismic base-isolation floor displacement vs. frequency ratio for different damping ratios

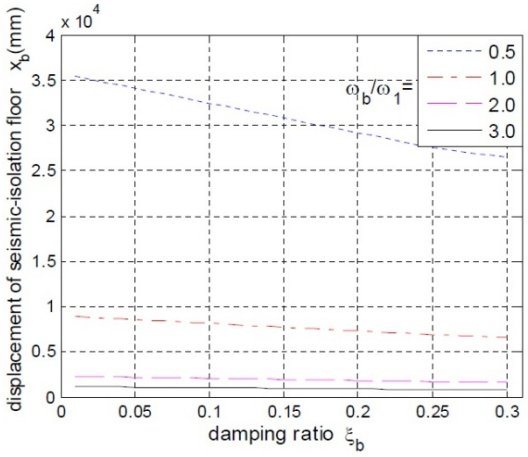

Fig. 7 Seismic base-isolation floor displacement vs. damping ratio for different frequency ratios

It can be observed that with the frequency ratio increasing, the base shear force ratio is monotonically increasing, while with the damping ratio increasing, the base shear force ratio is almost linearly decreasing, which illustrates that if the frequency ratio becomes smaller and the damping ratio becomes greater, the seismic base-isolation effect becomes larger. There is also an important issue in the design of seismic base-isolation floor, that is, the allowable displacement (under rare earthquake). In fact, the displacement of seismic base-isolation floor should be limited and has to meet the requirements of practical engineering.

Fig. 5 shows the relationship between seismic base-isolation floor displacement and frequency ratio, damping ratio. Compared with Fig. 2, it can be seen that the smaller the base shear ratio is (that is, the better seismic reduction effect), the larger the displacement of seismic base-isolation floor is. When the better seismic reduction effect is pursued, the displacement limit of seismic base-isolation floor should be also considered at the same time, which results in a problem of

constrained optimization. The relationships between seismic base-isolation floor displacement and frequency ratio for four different damping ratios are shown in Fig. 6, while the relationships between seismic base-isolation floor displacement and damping ratio for four different frequency ratios are shown in Fig. 7.

It is demonstrated that with the frequency ratio increasing, the displacement of seismic base-isolation floor is monotonically decreasing. When the frequency ratio is small, the displacement of seismic base-isolation floor changes greatly, while when the frequency ratio is large, the displacement of seismic base-isolation floor changes slowly. With the damping ratio increasing, however, the displacement of seismic base-isolation floor is almost linearly decreasing. When the frequency ratio is small, the enlargement of damping ratio has a great influence on the seismic base-isolation floor displacement, while when the frequency ratio is large, the enlargement of damping ratio has a little influence on the seismic base-isolation floor displacement.

It can be seen from Figs. 2-7 that to achieve a better seismic base-isolation effect, the damping ratio should be larger and the frequency ratio should be smaller. In addition, the displacement limit requirement of seismic base-isolation floor must be met.

The parameter optimization problem of seismic base-isolation structure is actually a problem of constrained optimization, so it can be described as the following mathematical model

$$\begin{cases} \min \beta \\ x_b \le x_{b\max} \\ 0 \le \xi_b \le \xi_{b\max} \\ m_b = cont \\ \Omega_1 \le \dfrac{\omega_b}{\omega_1} \le \Omega_2 \end{cases} \tag{33}$$

Taking into account the practical engineering situations and the characteristics of the example, $x_{b\max} = 200mm$, $\xi_{b\max} = 0.2$, $m_b = 400000kg$, $\Omega_1 = 0.5$, $\Omega_2 = 3.0$ are herein assumed. Then, the above parameter optimization problem can be resolved through any method of constrained optimization. Since Figs 2-7 show that the curves in figures are monotonically increasing or decreasing, this paper gives a more convenient and intuitive procedure combined with the example. The selection process for optimized parameters is as follows:

(1) Let $m_b = 400000kg$, and try to choose a larger damping ratio, that is $\xi_b = 0.2$;

(2) Let $x_b = 200mm$ and the corresponding frequency ratio can be obtained according to Fig. 6, that is $\omega_b / \omega_1 = 1.15$, so the three important parameters of seismic base-isolation floor can be determined.

(3) Once the frequency ratio is obtained, the corresponding base shear ratio can be determined through Fig. 3, which is $\beta = 0.59$, then the seismic reduction ratio is $\eta = (1-\beta)/1 = 41\%$.

4. Parametric studies

4.1 Influence of each mode on seismic base-isolation and optimal parameters

Table 3 Contribution for the base shear force of each mode

mode No.	base shear force (kN)		
	seismic-isolation structure	no seismic-isolation structure	vibration reduce value
1	674.47	1123.2	508.55
2	-0.6261	19.1	19.73
3~8	-0.0691	1.8	1.87

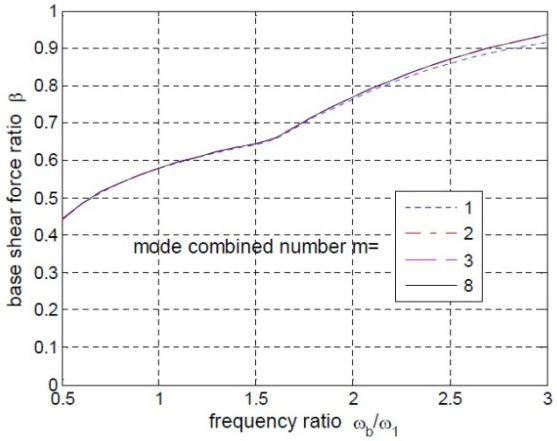

Fig. 8 Base shear force vs. frequency ratio for different mode combined numbers

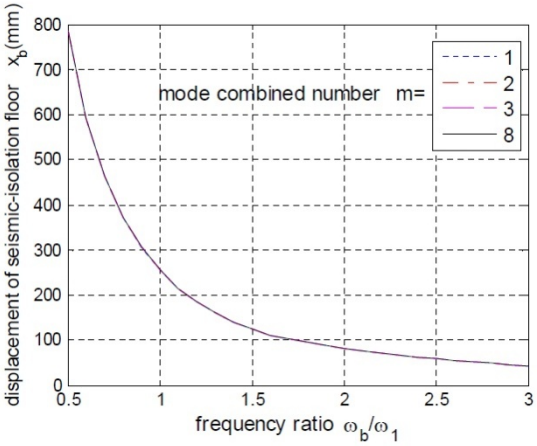

Fig. 9 Seismic base-isolation floor displacement vs. frequency ratio for different mode combined numbers

In order to see the influence degree of each mode on the seismic base-isolation, Table 3 lists the contribution of each mode to the base shear forces of seismic base-isolation structure and non-seismic base-isolation structure. It is demonstrated that the base shear force are primarily contributed by both first-order mode for seismic-isolation structure and non-seismic-isolation

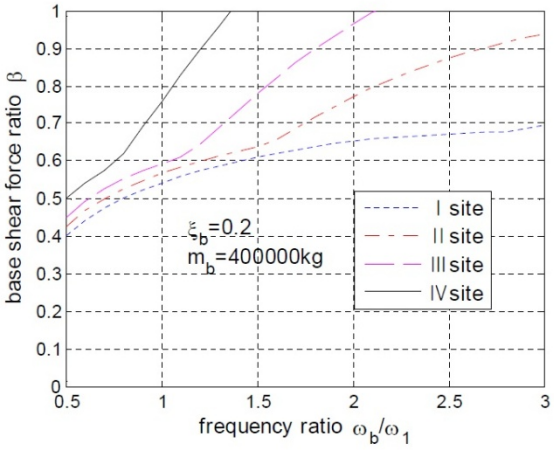

Fig. 10 Base shear force vs. frequency ratios for different site classifications

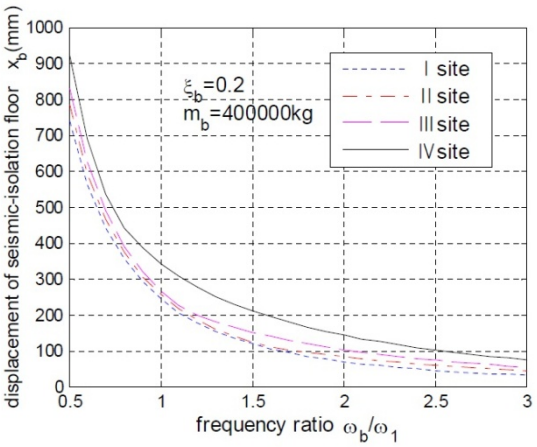

Fig. 11 Seismic base-isolation floor displacement vs. frequency ratio for different site classifications

structure.

Figs. 8 and 9 illustrate the relationship curves of base shear force ratio vs. frequency ratio, and the relationship curves of seismic base-isolation floor displacement vs. frequency ratio for different mode combined number of m=1, 2, 3, 8. As shown in Fig. 8, when the frequency ratio is small, the base shearing force is mainly contributed by the 1st mode, however, when the frequency ratio is large, the base shearing force is contributed by the 1st and 2nd modes. One can observe from Fig. 9 that the four curves are almost coincident, which illustrates that the number of mode combination has almost no effect on the result of parameter optimization.

4.2 Influence of site classification on seismic base-isolation and optimal parameters

In order to analyze the influence of site classification on the seismic base-isolation effect and optimization parameters, Figs. 10 and 11 respectively show the relationship curve of base shear

ratio β vs. frequency ratio, and the relationship curve of seismic base-isolation floor displacement vs. frequency ratio under different site classes: I, II, III and IV (the classification of design earthquake is the 1st group). The site classification and design earthquake can determine the characteristic period value, as shown in the code for seismic design of buildings (GB50011-2010) or Table B2 of Appendix B. It can be observed that softer the site soil is, worse the seismic base-isolation effect is when the optimal frequency ratio becomes larger. For the case of site class IV, the seismic base-isolation device may perhaps cause a negative impact, which needs to be careful.

5. Conclusions

Through the above analysis, the following conclusions can be drawn:

(1) The modified complex mode superposition design response spectrum method for earthquake effects calculation of seismic base-isolation structure is high-precision and convenient to engineering applications by applying complex modal decomposition technique, damping reduction factors and design response spectrum in seismic code.

(2) The proposed graphical approach is convenient to parameters optimization by analyzing the relationship between the base shear ratio of seismic base-isolation floor to non-seismic base-isolation one and frequency ratio-damping ratio, as well as the relationship between the seismic base-isolation floor displacement and frequency ratio-damping ratio. Some conclusions can be drawn: with the frequency ratio increasing, the base shear force ratio is monotonically increasing, while the seismic base-isolation floor displacement is almost linearly decreasing; with the damping ratio increasing, the base shear force ratio and seismic base-isolation floor displacement are almost linearly decreasing; with the damping ratio changing, the trends of base shear force ratio and seismic base-isolation floor displacement are consistent (i.e., the larger the damping ratio is, the better the seismic base-isolation effect is), however, with the frequency ratio changing, such trends are contradictory.

(3) For the seismic base-isolation structures, when the frequency ratio is small, the base shear force is mainly contributed by the 1st mode of superstructure, and when the frequency ratio is larger, the 2nd mode also makes some contributions. Moreover, the number of mode combination has almost no effect on the results of parameter optimization.

(4) The difference of earthquake site classification has great influence on the seismic base-isolation effects and optimized parameters: with the site soil becomes softer, the optimal frequency ratio becomes larger and the seismic-isolation effect becomes worse.

Acknowledgments

The work described in this paper was supported by both of the National Natural Science Foundation (51208524), Hunan Province Natural Science Foundation (12JJ4055), the Free Exploration Program of Central South University (201012200035), China Postdoctoral Science Foundation (20100471227), and Postdoctoral Science Foundation of Central South University. Any opinions and concluding remarks presented here are entirely those of the writers.

References

Alessandro, B. and Ileana, C. (2004), "Optimal design of base-isolators in multi-storey buildings", *Comput. Struct*., **82**(23-26), 2199-2209.

Balling, R.J., Pister, K.S. and Ciampi, V. (1983), "Optimal seismic-resistant design of a planar steel frame", *Earthq. Eng. Struct. D*., **11**(4), 541-556.

Buckle, I.G. and Mayes, R.L. (1990), "Seismic isolation: History, application, and performance-a world view", *Earthq. Spectra*, **6**(2), 161-201.

Cenk, A. and Henri, G. (2004), "A parametric study of linear and non-linear passively damped seismic isolation systems for buildings", *Eng. Struct*., **26**(4), 485-497.

Constantinou, M.C. and Tadjbakhsh, I.G. (1983), "Probabilistic optimum base isolation of structures", *J. Struct. Div.- ASCE*, **109**(3), 676-689.

Constantinou, M.C. and Tadjbakhsh, I.G. (1984), "The optimum design of a base isolation system with frictional elements", *Earthq. Eng. Struct. D*., **12**(2), 203-214.

Elishakaff, I. and Lyon, R.H. (1986), *Random vibration-status recent developments*, Elsvier.

Eurocode. (2004), *Design of structures for earthquake resistance*, European committee for standardization (CEN), Brussels.

Fan, F.G., Ahmadi, G., Mostaghel, N. and Tadjbakhsh, I.G. (1991), "Performance analysis of aseismic base-isolation systems for a multi-story building", *Soil Dyn. Earthq. Eng*., **10**(3), 152-171.

Fawzy, I. and Bishop, R.E.D. (1976), "On the dynamics of linear no conservative systems", *Proc. Roy. Soc*, London, Ser.A, 325-352.

GB50011 (2010), *Code for seismic design of buildings*, National Standard of the People's Republic of China.

Gupta, A.K. and Jaw, J.W. (1986), "Response spectrum method for nonclassically damped systems", *Nucl. Eng. Des*., **91**(2), 161-169.

Heaton, T.H., Hall, J.F., Wald, D.J. and Halling, M.W. (1995), "Response of high rise and base-isolated buildings to a hypothetical Mw 7.0 blind trust earthquake", *Sci*., **267**, 206-211.

Hong, W.K. and Kim, H.C. (2004), "Performance of a multi-story structure with a resilient-friction base-isolation system", *Comput. Struct*., **82**(27), 2271-2283.

Horisberger, H.P. and Belanger, P.R. (1974), "Solution of the optimal output feedback problem by conjugate gradients", *IEEE T. Automat. Contr*., **19**(4), 434-435.

Igusa, T., Der Kiureghian, A. and Sackman, J.L. (1984), "Modal decomposition method for stationary response of non-classically damped systems", *Earthq. Eng. Struct. D*., **12**(1), 121-136.

Jangid, R.S. and Datta, T.K. (1995), "Performance of base isolation systems for asymmetric building subject to random excitation", *Eng. Struct*., **17**(6), 443-454.

Kim, H.S. and Roschke, P.N. (2007), "GA-fuzzy control of smart base isolated benchmark building using supervisory control technique", *Adv. Eng. Softw*., **38**(7), 453-465.

Komodromos, P. (2000), *Seismic isolation for earthquake resistant structures*, Southampton: WIT Press.

Lin, Y.Y. and Chang, K.C. (2003), "Study on damping reduction factor for buildings under earthquake ground motions", *J. Struct. Eng.-ASCE*, **129**(2), 206-214.

Matsagar, V.A. and Jangid, R.S. (2004), "Influence of isolator characteristics on the response of base-isolated structures", *Eng. Struct*., **26**(12), 1735-1749.

Mahendra, P.S. and Barbara, E.M. (1986), "Mode acceleration-based response spectrum approach for nonclassically damped structures", *Soil Dyn. Earthq. Eng*., **5**(4), 226-233.

Naeim, F. and Kelly, J.M. (1999), *Design of seismic isolated structures-from theory to practice*, New York: John Wiley & Sons, Inc.

Skinner, R.I., Robinson, W.H. and McVerry, G.H. (1993), *An introduction to seismic isolation*, Chichester: Wiley.

Takewaki, I. (2005), "Uncertain-parameter sensitivity of earthquake input energy to base-isolated structure", *Struct. Eng. Mech*., **20**(3), 347-362.

Takewaki, I. (2008), "Robustness of base-isolated high-rise buildings under code-specified ground motions", *Struct. Des. Tall Spec*., **17**(2), 257-271.
Takewaki, I. and Fujita, K. (2009), "Earthquake input energy to tall and base-isolated buildings in time and frequency dual domains", *J. Struct. Des. Tall Spec*., **18**(6), 589-606.
Yang, J.N., Sarkani, S. and Long, F.X. (1990), "A response spectrum approach for seismic analysis of nonclassically damped structures", *Eng. Struct*., **12**, 173-184.
Yoshi, S., Shin'ichiro, T., Hiroaki, M. and Noriaki, S. (1999), "An optimal design of the base-isolated device by using genetic algorithm-a proposal of a method and some examples of its application", *Proceedings of International Conference on Computer Aid Optimal Design of Structures*, Computational Mechanics Publications. Orlando, Florida, USA, 225-234.
Zhou, X.Y. and Han, M. (1996), "Optimum design of reuben-friction-slide base isolation system for low cost buildings", *Proc. 11th World Conference on Earthquake Engineering*, Acapulco Mexico, 24-29.
Zhou, X.Y., Yu, R.F. and Dong, L. (2004), "The complex-complete-qua-draft- combination (CCQC) method for seismic responses of non-classically damped linear MDOF system", *Proc. 13th World Conference on Earthquake Engineering*, 848, Vancouver, Canada, 1-6.

IT

Appendix A

The expressions of the responses is

$$q_j(t)=\sum_{k=1}^{m+1}(2E_{jk}\eta_k(t)+2G_{jk}\dot{\eta}_k(t)) \qquad (j=1\sim m) \tag{A.1a}$$

$$x_b(t)=\sum_{k=1}^{m+1}(2\tilde{E}_k\eta_k(t)+2\tilde{G}_k\dot{\eta}_k(t)) \tag{A.1b}$$

According to the stationary random vibration theory, the mean square value of response $q_j(t)$ is (the solution process for $x_b(t)$ is similar to $q_j(t)$)

$$\mathrm{E}\left[q_j{}^2(t)\right]=\mathrm{E}\left[\sum_{k=1}^{m+1}\left(2E_{jk}\eta_k(t)+2G_{jk}\dot{\eta}_k(t)\right)\right]=\mathrm{E}\left[\sum_{k=1}^{m+1}2E_{jk}\eta_k(t)+\sum_{k=1}^{m+1}2G_{jk}\dot{\eta}_k(t)\right]^2 =$$

$$\sum_{k=1}^{m+1}\sum_{l=1}^{m+1}\left[2E_{jk}\cdot 2E_{jl}\cdot\mathrm{E}\left[\eta_k(t)\cdot\eta_l(t)\right]+2E_{jk}\cdot 2G_{jl}\cdot\mathrm{E}\left[\eta_k(t)\cdot\dot{\eta}_l(t)\right]+2G_{jk}\cdot 2G_{jl}\cdot\mathrm{E}\left[\dot{\eta}_k(t)\cdot\dot{\eta}_l(t)\right]\right]$$

$$=\sum_{k=1}^{m+1}\sum_{l=1}^{m+1}\left(2E_{jk}\cdot 2E_{jl}\cdot I_{kl}^{DD}\right)+2\cdot\sum_{k=1}^{m+1}\sum_{l=1}^{m+1}\left(2E_{jk}\cdot 2G_{jl}\cdot I_{kl}^{DV}\right)+\sum_{k=1}^{m+1}\sum_{l=1}^{m+1}\left(2G_{jk}\cdot 2G_{jl}\cdot I_{kl}^{VV}\right)(j=1\sim m) \tag{A.2}$$

in which

$$I_{kl}^{DD}=\int_{-\infty}^{+\infty}H_k(i\omega)H_l(-i\omega)S_g(\omega)\mathrm{d}\omega \tag{A.3a}$$

$$I_{kl}^{DV}=\int_{-\infty}^{+\infty}i\omega H_k(i\omega)H_l(-i\omega)S_g(\omega)\mathrm{d}\omega \tag{A.3b}$$

$$I_{kl}^{VV}=\int_{-\infty}^{+\infty}\omega^2 H_k(i\omega)H_l(-i\omega)S_g(\omega)\mathrm{d}\omega \tag{A.3c}$$

where $S_g(\omega)$ is the spectral density of ground motion; $H_k(i\omega)$ ($H_l(-i\omega)$) is the transfer function of structure, and it can be written as

$$H_k(i\omega)=-\frac{1}{\tilde{\omega}_k^2-\omega^2+2i\tilde{\xi}_k\tilde{\omega}_k\omega} \tag{A.4}$$

Assumed that the ground motion $\ddot{x}_g(t)$ is a zero-mean stationary white noise process, there is

$$\mathrm{E}\left[\ddot{y}_{gk}(\tau)\ddot{y}_{gl}(s)\right]=2\pi S_0\delta(\tau-s) \tag{A.5}$$

where $\delta(\tau-s)$ is Dirac delta function; S_0 is the intensity parameters when ground motion is

looked on as white noise process.

Elishakaff and Lyon (1986) deduced the mode correlative coefficients by the integral method provided in appendix, which is

$$\rho_{kl}^{DD} = \frac{I_{kl}^{DD}}{\sqrt{I_{kk}^{DD}}\sqrt{I_{ll}^{DD}}} = 8\sqrt{\tilde{\xi}_k \tilde{\xi}_l \tilde{\omega}_k \tilde{\omega}_l}\,(\tilde{\xi}_k \tilde{\omega}_k + \tilde{\xi}_l \tilde{\omega}_l)\tilde{\omega}_k \tilde{\omega}_l / \Gamma_{kl} \tag{A.6a}$$

$$\rho_{kl}^{VD} = \frac{I_{kl}^{VD}}{\sqrt{I_{kk}^{VV}}\sqrt{I_{ll}^{DD}}} = 4\sqrt{\tilde{\xi}_k \tilde{\xi}_l \tilde{\omega}_k \tilde{\omega}_l}\,(\tilde{\omega}_l^2 - \tilde{\omega}_k^2)\tilde{\omega}_l / \Gamma_{kl} \tag{A.6b}$$

$$\rho_{kl}^{VV} = \frac{I_{kl}^{VV}}{\sqrt{I_{kk}^{VV}}\sqrt{I_{ll}^{VV}}} = 8\sqrt{\tilde{\xi}_k \tilde{\xi}_l \tilde{\omega}_k \tilde{\omega}_l}\,(\tilde{\xi}_k \tilde{\omega}_l + \tilde{\xi}_l \tilde{\omega}_k)\tilde{\omega}_k \tilde{\omega}_l / \Gamma_{kl} \tag{A.6c}$$

$$\Gamma_{kl} = (\tilde{\omega}_k^2 - \tilde{\omega}_l^2)^2 + 4\tilde{\xi}_k \tilde{\xi}_l \tilde{\omega}_k \tilde{\omega}_l (\tilde{\omega}_k^2 + \tilde{\omega}_l^2) + 4(\tilde{\xi}_k^2 - \tilde{\xi}_l^2)\tilde{\omega}_k^2 \tilde{\omega}_l^2 \tag{A.6d}$$

Then the absolute maximums of $q_j(t)$ （see Eq.(A.2)）can be written as

$$\left|q_j\right|_{\max} = \sqrt{S_1 + S_2 + S_3} \quad (j = 1 \sim m) \tag{A.7}$$

in which

$$S_1 = \sum_{k=1}^{m+1} \sum_{l=1}^{m+1} 2E_{jk} \cdot 2E_{jl} \cdot \rho_{kl}^{DD} \cdot S_{dk} \cdot S_{dl} \tag{A.8a}$$

$$S_2 = 2\sum_{k=1}^{n+1} \sum_{l=1}^{n+1} 2E_{jk} \cdot 2G_{jl} \cdot \rho_{kl}^{VD} \cdot S_{dk} \cdot S_{vl} \tag{A.8b}$$

$$S_3 = \sum_{k=1}^{n+1} \sum_{l=1}^{n+1} 2G_{jk} \cdot 2G_{jl} \cdot \rho_{kl}^{VV} \cdot S_{dk} \cdot S_{vl} \tag{A.8c}$$

$$\rho_{kl}^{DD} = 8\sqrt{\tilde{\xi}_k \tilde{\xi}_l \tilde{\omega}_k \tilde{\omega}_l}\,(\tilde{\xi}_k \tilde{\omega}_k + \tilde{\xi}_l \tilde{\omega}_l)\tilde{\omega}_k \tilde{\omega}_l / \Gamma_{kl} \tag{A.8d}$$

$$\rho_{kl}^{VD} = 4\sqrt{\tilde{\xi}_k \tilde{\xi}_l \tilde{\omega}_k \tilde{\omega}_l}\,(\tilde{\omega}_l^2 - \tilde{\omega}_k^2)\tilde{\omega}_l / \Gamma_{kl} \tag{A.8e}$$

$$\rho_{kl}^{VV} = 8\sqrt{\tilde{\xi}_k \tilde{\xi}_l \tilde{\omega}_k \tilde{\omega}_l}\,(\tilde{\xi}_k \tilde{\omega}_l + \tilde{\xi}_l \tilde{\omega}_k)\tilde{\omega}_k \tilde{\omega}_l / \Gamma_{kl} \tag{A.8f}$$

$$\Gamma_{kl} = (\tilde{\omega}_k^2 - \tilde{\omega}_l^2)^2 + 4\tilde{\xi}_k \tilde{\xi}_l \tilde{\omega}_k \tilde{\omega}_l (\tilde{\omega}_k^2 + \tilde{\omega}_l^2) + 4(\tilde{\xi}_k^2 - \tilde{\xi}_l^2)\tilde{\omega}_k^2 \tilde{\omega}_l^2 \tag{A.8g}$$

When it comes to the absolute maximal displacement of seismic base-isolation floor, i.e.,

$|x_b|_{\max}$, the Eq.(A.7) is also applicable and the E_{jk} and G_{jk} in Eq.(A.8) should be replaced by $\tilde{E}_k$ and $\tilde{G}_k$, respectively.

Appendix B

a: seismic influence coefficient; $a_{\max}$: maximum value of seismic influence coefficient; η_1: adjusting factor of slope for the linear decrease section; γ: power index; T_g: characteristic period; η_2: damping adjustment factor and T: structural natural periods.

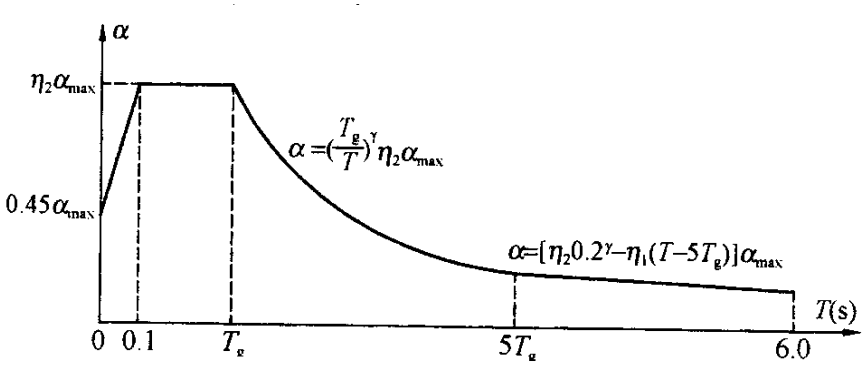

Fig. B1 Seismic influence coefficient curve

Table B1 Maximum value of horizontal seismic influent coefficient

Earthquake influence	Intensity 6	Intensity 7	Intensity 8	Intensity 9
Frequently earthquake	0.04	0.08（0.12）	0.16(0.24)	0.32
Rarely earthquake	0.28	0.50（0.72）	0.90(1.20)	1.40

Note: the values in the brackets are separately used for where the design basic seismic acceleration is 0.15 g and 0.30 g.

Table B2 Characteristic period value (*s*)

Design earthquake group	Site-class			
	Ⅰ	Ⅱ	Ⅲ	Ⅳ
1st Group	0.25	0.35	0.45	0.65
2nd Group	0.30	0.40	0.55	0.75
3rd Group	0.35	0.45	0.65	0.90